Multi-scale foam : 3D structure/compressive behaviour relationship of agglomerated cork

Louise Le Barbenchon, Jérémie Girardot, Jean-Benoit Kopp, Philippe Viot

▶ **To cite this version:**

Louise Le Barbenchon, Jérémie Girardot, Jean-Benoit Kopp, Philippe Viot. Multi-scale foam : 3D structure/compressive behaviour relationship of agglomerated cork. Materialia, 2019, 5, pp.100219. hal-02405511

HAL Id: hal-02405511
https://hal.science/hal-02405511

Submitted on 11 Dec 2019

HAL is a multi-disciplinary open access archive for the deposit and dissemination of scientific research documents, whether they are published or not. The documents may come from teaching and research institutions in France or abroad, or from public or private research centers.

L'archive ouverte pluridisciplinaire **HAL**, est destinée au dépôt et à la diffusion de documents scientifiques de niveau recherche, publiés ou non, émanant des établissements d'enseignement et de recherche français ou étrangers, des laboratoires publics ou privés.

Multi-scale foam : 3D structure/compressive behaviour relationship of agglomerated cork

Louise Le Barbenchon*, Jérémie Girardot, Jean-Benoît Kopp, Philippe Viot

Arts et Métiers ParisTech, CNRS, I2M Bordeaux, Esplanade des Arts et Métiers, Talence Cedex F-33405, France

Keywords:
Multi-scale microstructure
Cellular material
Cork agglomerate
X-ray microtomography
Mechanical behaviour

A B S T R A C T

This study focuses on the microstructural aspects of a cork-based by-product known as agglomerated cork and its influence on the compressive mechanical behaviour. The material consists in granulates of a natural polymeric foam - cork - mixed together with a small quantity of a bio-sourced resin.

Optical and scanning electron microscopy (SEM) are first used to investigate on the bead geometry and placement and interfaces arrangement. Then X-ray computed tomography allows to study the spatial arrangement of agglomerated cork microstructure and hence to complete and confirm 2D observations. 2D and 3D observations show a transverse anisotropic material which is confirmed by the mechanical tests. SEM pictures demonstrate an intricate and heterogeneous material. Microtomography confirms the presence of macroporosities between cork granulates having a mean volume around 0.1 mm^3. Cork cell specific geometry is also confirmed. The volume of those cells lies around 10^{-5} mm^3. Finally quasi-static compression tests are run to establish a link between microstructure and mechanical behaviour thanks to digital image correlation (DIC). Cork agglomerate demonstrates strong strain localisation at its surface caused by its multi-scale structure.

1. Introduction

Because of emerging concerns about global warming and thus about the carbon footprint, the demand for bio-sourced materials is currently increasing. Cork material being a natural polymeric foam, it presents a unique set of properties (fire resistant, energy absorbing, phonic isolation,...). It is then an excellent candidate for a large set of applications.

Cork comes from the bark of the oak tree *Quercus Suberus L.* growing in areas like Portugal, Spain or certain parts of China. Europe produces 80% of the world's cork and almost three quarter of them come from Portugal [1]. It is a very unique material due to its low density - around 0.17 -, great elasticity, chemical stability, its no permeability to liquid and gases and its resistance to fire [2]. Cork is used for centuries, first by the Romans in sandals or stoppers for amphorae. Its most popular application - stoppers for glass bottles - was perfected in the 18th century in a Benedictine Abbey in Hautvillers, France [2]. Cork by-products are today mainly developed for their thermal insulation and acoustic properties [3]. Due to its cellular microstructure, cork absorbing properties for dynamic loading are now being considered for impact-absorbing applications as core material in sandwich structures [4]. Ranging from the container for the transport of sensible pieces to sports items and including lightweight aeronautic components, a wide range of applications is foreseen [1,5].

To decrease the variability caused by environmental dependency (weather, growing place, harvest season) [6,7], a cork by-product - agglomerated cork- is preferred for mechanical applications. It also allows to overstep the anisotropy of natural cork by randomly arranging cork cell orientation and to mold pieces with a more complex geometry. For 10 years, few studies investigated on the mechanical behaviour of such materials under quasi-static and impact loadings [8–12]. Giving its considered applications, they focused on the compressive behaviour of cork agglomerates. They demonstrated the influence of the mean strain rate, cork granulates size, the type of resin or the material density on the absorbed energy, contact force maximum or the acceleration peak maximum.

However the microstructure of this material is still not fully reviewed, even if it could strongly influence its mechanical behaviour and its specific strain mechanisms. Only the microstructure of natural cork has been quite studied. SEM observations of natural cork give information concerning the cell specific geometry [2] and surface distribution of each direction [13]. Concerning the spatial organisation, only the macroscopic defects of natural cork, like lenticular channel (also called lenticels) or ants galeries, were investigated by using either neutron tomography [14] (for a spatial resolution of 200 μm), Compton tomography [15] or X-ray tomography [16,17] (spatial resolution of 2 mm and 50 μm). Those techniques were used to study the correlation between

* Corresponding author.
E-mail address: louise.le_barbenchon@ensam.eu (L. Le Barbenchon).

https://doi.org/10.1016/j.mtla.2019.100219

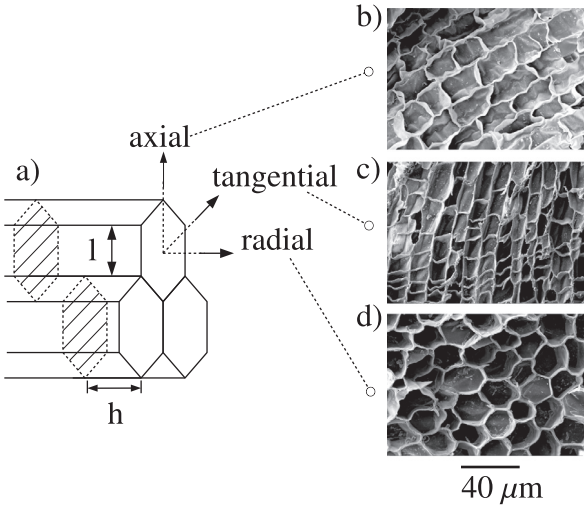

Fig. 1. (a) Natural cellular disposition of cork. (b) Axial direction. (c) Tangential direction. (d) Radial direction. SEM Pictures.

cork quality (given by surface analysis) and internal defects of cork stoppers. It was shown cork quality matches with macroscopic defects population. Furthermore X-ray microtomography at a higher spatial resolution (50 μm) was well suited to focus on the lenticular channels quantification and their structures [17]. Internal feature and contrast mechanisms were also studied with synchrotron X-Rays at several tensions [18]. However only important cracks and lenticels could be spotted.

Agglomerated cork was itself not studied with quantitative tools while recent observations using microtomography proved it was well suited to investigate for example on the 3D structure of foams at several scales [19–21]. It has been used to study the complex arrangement of the cells of cellular materials of metals, polymers and natural foams like bone.

This work has two aims. The first one is to study with several techniques the microstructure of cork agglomerates and to give the first quantitative data at several scales (cells and beads). Such microstructural study is one of the first concerning multi-scales foams like agglomerated cork. The post-processing is then detailled in the Material & Methods part. The other goal is to investigate the global response of cork under compression and to link it to the microstructure observations. It was indeed already done for natural cork [22] or other cellular materials [23] but not for agglomerated cork.

First optical microscopy is used to understood geometrical aspect at the agglomerate scale. Then scanning electronic microscopy permits to observe not only beads organisation and interfaces between them but also cork cells orientation. Finally as those two techniques are invasive and allow only to access to the surface of the sample, X-ray microtomography is used to verify assumptions made with previous observations. Quasi-static uniaxial compressive tests and digital image correlation are also run in order to discuss about microstructural effects on the mechanical behaviour.

2. Material & methods

2.1. Materials

Cork is a natural polymeric foam which displays a closed-cell structure [2]. It is formed by small prismatic cells (with an approximated length h of 40 μm) disposed in successive layers (Fig. 1) exhibiting a relatively homogeneous honeycomb microstructure. Suberin, a polymeric substance, is the major component of cork cell walls. The other are lignin, cellulose and hemicelluloses [24].

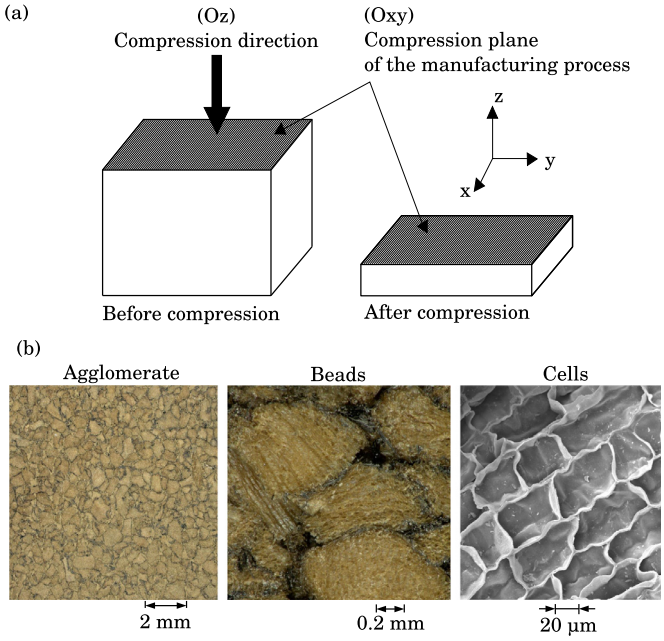

Fig. 2. Agglomerated cork: a multi-scale material influenced by the manufacturing process. (a) Orientations resulting from the process. (b) Different observation scales demonstrating the multi-scale structure of agglomerated cork. At the agglomerate and bead scales, pictures are taken with a light microscope. Cells scale is illustrated with a SEM image of cork cells observed in the axial direction.

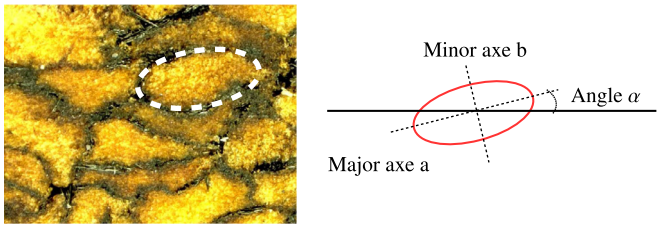

Fig. 3. Geometrical approximation for a cork granulate and ellipse parameters.

To obtain agglomerated cork, natural cork is ground and sieved to classify it by size. In this study, small beads (ø = 0.5 - 1 mm) are mixed together with a thermoset furan resin (ρ_{resin}= 1128.5 kg m^{-3}). It is then uni-axially compressed into a 1000×500×150 mm^3 block at a 0.39 density. This compression induces a preferential orientation that will be further investigated in this article. Fig. 2a shows the two directions induced: directions in the (Oxy) plane will be arbitrarily called in-plane directions and (Oz) direction will be called out-of-plane direction. Afterwards the crossing is made in an autoclave. Slab are then machined from the block.

Cellular solids are often described by their relative density ρ^*/ρ_s. The density of the cellular material is ρ^* and ρ_s is the density of the solid from which the cell walls are made. With ρ_s = 1150 kg m^{-3} [2], the relative density of agglomerated work studied is this article is around 0.34.

2.2. Light microscopy

The material is first studied with an optical microscope Keyence at a magnification of ×20. The surface of several samples is observed. With the ImageJ free-software, picture analysis on the resulting pictures is operated by thresholding only the beads. Erosion and dilatation operations are then used to separate each bead. Finally particle analysis is done by simplifying granulates by ellipses (Fig. 3). Geometrical parameters of those ellipses are then used to calculate the aspect ratio (AR) and

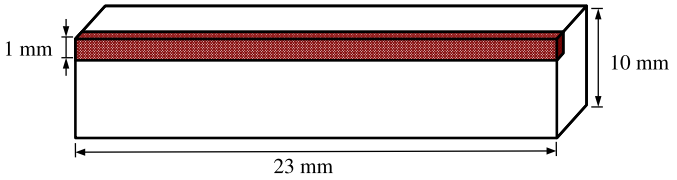

Fig. 4. Microtomography samples. A first square-based prism is cut for a first tomography analysis. A smaller one is then cut inside for a second microtomography analysis (hatched prism).

the granulates orientation α. Aspect ratio is a shape factor obtained by dividing the minor axis length by the major one (AR = a/b). The more AR is close to 1 and the more the particle tends to be circular.

2.3. SEM observations

SEM samples are cut with a razor blade replaced for each cut in order to damage as less as possible the cell walls [2,25]. Each cubic sample is cut over-size and then trimmed to the final size (roughly 5 mm sides). Samples are then lightly coated with conductive gold to allow electronic conduction at the sample surface. The device used was a Cressington 108 auto. The gold layer is supposed constant on the sample surface. Samples are then observed with a SEM (Zeiss EVO HD 15). An accelerated tension of 10 keV is used with a current of 100 pA. Both directions of the cork are studied.

2.4. X-ray microtomography

The two previous methods involve only surface analysis and do not allow full description of the complex microstructure. A bias could also be introduced by cutting steps (cell distortion, interfaces damage,...) because of the very low density and high porosity of the material. That is why tomography is undertaken.

The general principle of the X-ray microtomography technique has been described in many articles like by Maire et al [26].

It requires a X-ray source, a rotation stage and a radioscopic detector. To obtain a complete analysis, for a large number of angles, X-ray absorption radiography of the sample is made. A final computed reconstruction step is required to produce a three dimensional map of the local absorption coefficients in the material which gives a picture of the structure. The scale of the resolution of the setup used is a voxel which corresponds to a 3D pixel.

One sample is used for two X-ray resolutions (Fig. 4). The first 8.5 μm/voxel resolution gives the structure at the granulate scale. The acceleration voltage and current of the X-rays were set at respectively 80 kV and 100 μA. After this first analysis, a sample is cut from it at smaller dimensions to obtain a 2.5 μm/voxel resolution to study the cell scale. This time the acceleration voltage and current of the X-rays were set at respectively 70 kV and 220 μA.

2.5. 3D image analysis

Post-treatment analysis algorithm of tomography data is done thanks to the Amira-Avizo software to calculate quantitative parameters and obtain the 3D reconstruction. Morphometric parameters were calculated using a prismatic sub-volume of the original object imaged, referred herein to as the volume of interest (VOI). For the beads study, the selected VOI was located at the centre of the specimen to eliminate any edge effects, artefacts and damages from sample cutting. In order to study the cork cells, three VOI were selected inside a bead to avoid any effects caused by the interfaces. Each VOI was then filtered and segmented according to the steps described in the following parts.

The uncertainty of acquisition technique itself seems much smaller than the one due to the data analysis. Especially the image segmentation, which is one of the major difficulties [27]. However it seems there is no established technique to evaluate how the segmentation technique is accurate. Yet in the case of cork, the natural variability of the material [6] and the variability due to the process (beads grinding) are supposed much bigger than all the other uncertainties. This is then the statistical distribution of all the morphometric parameters that will be considered in this work.

2.5.1. Large sample

For the first sample, a simple thresholding on raw images does not permit to access to morphometric parameters immediately. Indeed beads are made of cork cells containing voids. Therefore it causes too much noise to allow a good segmentation of cork granulates (Fig. 5a).

First of all a histogram equalisation (Fig. 5b) is used to enhance the contrast by redistributing the intensity values from 16 bits images (grey levels between 0 and 65535) to 8 bits images (grey levels between 0 and 255). The histogram is computed between the minimum and the maximum of the image grey levels.

Then a median filter is applied (Fig. 5c). This numerical filter works by moving through the image pixel by pixel, replacing each value with the median value of neighbouring pixels.

After that a simple thresholding is used to select either porosities or granulates (Fig. 5d). Then an opening (an erosion followed by a dilatation with a structuring element like a cube or a disc) [28] is done to suppress irregularities or single voxels (Fig. 5e).

Finally a segmentation is operated in order to fully separate each bead thanks to topographic conditions (Fig. 5f). After this segmentation, a single label can be associated with each bead (Fig. 5f). Segmentation is not used on the porosities.

The 3D segmentation method is itself divided into three main steps [21]. First, a distance map image is computed (Fig. 5g) and the position of the ultimate eroded sets, called markers, is determined [29,30]. The Chamfer distance is used in this case. The right markers are then selected by topographic conditions. Here the H-maxima algorithm is used on the inversed distance map to merge regional maximums with a contrast coefficient criterion h (Fig. 5h). Finally, the watershed is constructed from these markers with the help of the distance function [31] (Fig. 5i). The result gives separating lines that can be subtracted to the initial binary image.

From the post-treatment of almost the whole sample, near 9000 beads were studied. The sample is then large enough be representative. Volume, orientation and sphericity of cork beads and porosities were the main interesting data. Beads having a volume smaller than 0.002 mm^3 were here not considered being associated with noise. Orientation is characterised by the two angles θ and ϕ usually used for spherical coordinates. Sphericity ψ measures how closely the shape of an object approaches a mathematically "perfect" sphere. It is calculated according to Eq. (1), with V_p, the volume of the particle and A_p, the surface area of the particle. The nearer to 1, the closer to a sphere.

$$\psi = \frac{\pi^{\frac{1}{3}}(6V_p)^{\frac{2}{3}}}{A_p}. \tag{1}$$

2.5.2. Small sample

On the other hand, no filter is needed for the smaller sample post-processing because of the difference of density between cork cells walls and voids inside cells. A simple threshold is applied to generate a binary image of the gaseous phase.

After that, in order to extract morphometric parameters, the same morphological operations as for the large resolution sample are used (Fig. 6). Table 1 resumes input entered to study either beads or porosities and cells.

From the post-treatment of different areas in cork granulates, almost 1400 cells were studied. The sample seems also large enough to be representative of the microstructure at the cell scale.

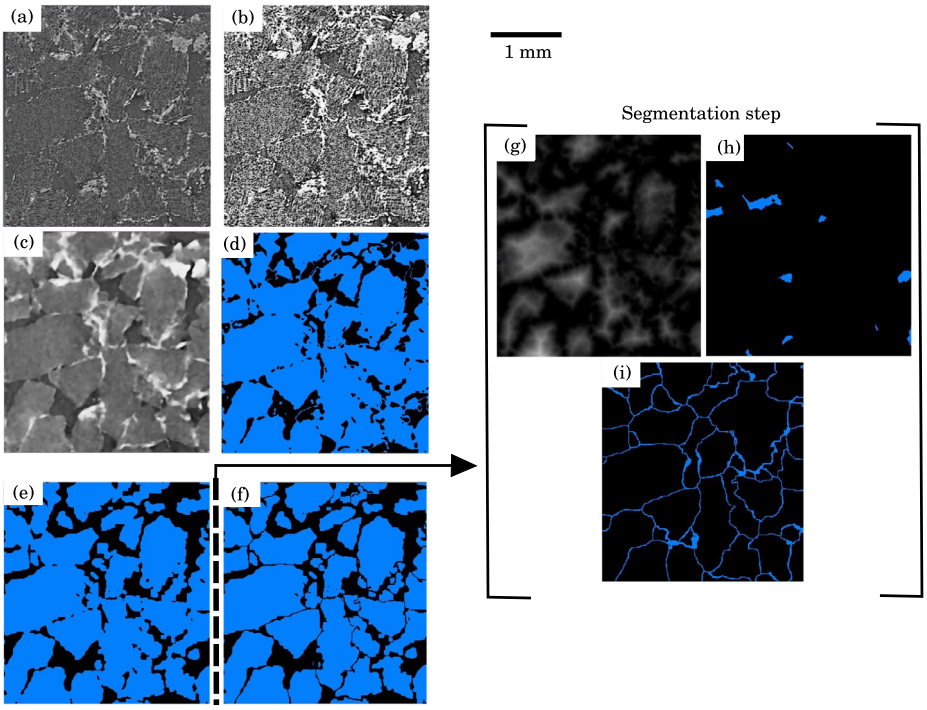

Fig. 5. Post-treatment process of X-ray microtomograhy data. (a) Raw picture. (b) Histogram equalisation. (c) Median filter. (d) Thresholding. (e) Opening. (f) Segmentation. Steps of the segmentation operation. (g) Inversed Chamfer distance map. (h) Marker selectionned thanks to H-maxima technique. (i) Watershed lines obtained with a marker-based segmentation.

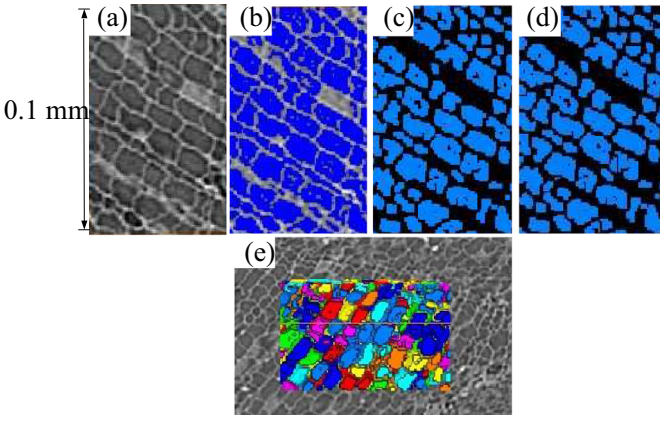

Fig. 6. Process to obtain 3D information on cork cells. (a) Raw image. (b) Thresholding. (c) Opening. (d) Separation. (e) Volume rendering.

Table 1
Data of the post-processing of X-ray microtomography images.

Operation	Type	Beads	Pores	Cells
Median filter	Iterations	7	7	–
Thresholding	Range selected	96–169	0–96	0–26270.5
Opening	Structuring element (iteration)	Cubes (5)	Disc (2)	Disc (2)
Distance map	Distance between 2 voxels max/mean/min 3D connexity	1/1.414/1.73	same	same
H-maxima	Merging coefficient	6	4	4

2.6. Quasi-static compression tests

As cork is a cellular material, its absorbing properties for compressive loading are now being considered for impact-absorbing applications as core material in sandwich structures [4]. To be able to relate microstructure observations with mechanical behaviour, quasi-static compressive tests are run to propose simple data for further investigations. Digital image correlation (DIC) is used to precisely describe strain evolution during a compressive load.

2.6.1. Experimental protocol

$20 \times 20 \times 20\,\text{mm}^3$ samples are cut from large slabs of agglomerated cork. An electromechanical traction/compression machine (Zwick Roell 250 from Allround-Line) with a load cell capacity of 250 kN is used. The loading speed is set at 0.05 mm min^{-1}, 5 mm min^{-1} and 500 mm min^{-1} corresponding to an average strain rate of 4.2 10^{-5} s^{-1}, 4.2 10^{-3} s^{-1} and 4.2 10^{-1} s^{-1}, respectively. Mechanical behaviour of the three main directions spotted with optical microscopy is investigated. They are called out-of-plane (Oz), in-plane 1 (Ox) and in-plane 2 (Oy). Six samples per direction are tested.

To study the relationship between microstructure and mechanical behaviour, pictures are taken at a 1 Hz frequency during compressive loadings at 5 mm min^{-1} with a Canon EOS 5D thanks to a square signal given by a GBF.

Some cyclic compression tests are undertaken at an average strain-rate of 4.2 10^{-3} s^{-1}. Samples are unloaded to zero force after each incremental 1 mm displacement. Six cycles are operated. Two samples for both in-plane and out-of-plane direction are tested.

2.6.2. Post-processing of the compression tests

From the force/displacement data, stress/strain curves are deducted by calculating nominal stress ($\sigma = \frac{F}{S_0}$) and true strain ($\epsilon = \ln\frac{l_0 - l}{l}$). Poisson's ratio of cork being near 0 [2], the section did not change during the compression test.

To obtain the Young's modulus, the curve is fitted with a seven degree polynomial. The end of the linear part of the curve is found with its second derivative minimum. A one degree polynomial is then calculated between $\epsilon = 0.01$ and this point. Its slope corresponds to the Young's modulus given in this article. However the Young's modulus being still not precisely defined, moreover for cellular materials [32], others parameters are needed to characterize agglomerated cork.

To study the plateau stage an energy absorption efficiency approach is adopted [33]. The energy absorption efficiency [34] is defined by

$$\eta(\varepsilon) = \frac{1}{\sigma(\varepsilon)} \int_0^{\varepsilon} \sigma(\varepsilon)\, \mathrm{d}\varepsilon. \tag{2}$$

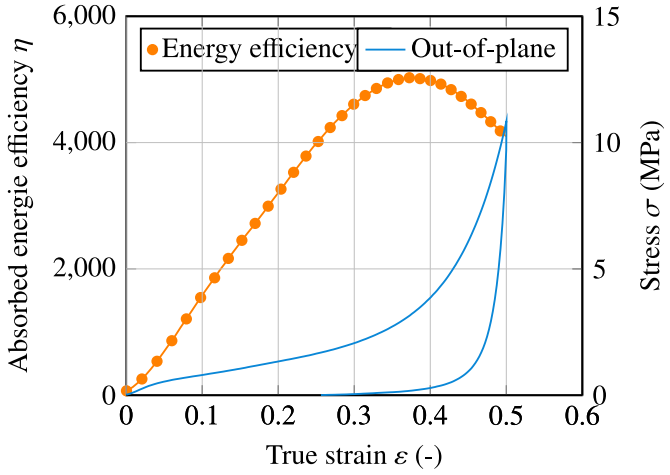

Fig. 7. Experimental curve showing the energy absorption efficiency depending on the strain for agglomerated cork compressed in the out-of-plane direction at 5 mm min^{-1}.

The maximum energy absorption efficiency corresponds to the densification initiation strain ε_{d0} so that

$$\left.\frac{d\eta(\varepsilon)}{d\varepsilon}\right|_{\varepsilon=\varepsilon_{d0}} = 0. \quad (3)$$

Fig. 7 illustrates the absorbed energy efficiency variation along the strain.

Absorbed energy before densification which corresponds to the sum of dissipated and elastic energies is then calculated. It is obtained by integrating along the displacement using the composite trapezoidal rule. Plateau absorbed energy density at densification initiation is calculated by integrating until $\varepsilon = \varepsilon_{d0}$ and by dividing the energy found by the sample volume. For the Young's modulus, the densification initiation strain and the absorbed energy at densification, the dispersion is quantified. The mean deviation calculated corresponds to the average of the absolute differences in comparison to the arithmetic average.

With pictures taken during compressive tests, DIC is operated. Indeed cork agglomerates demonstrate a specific texture and do not require a speckled pattern [12]. The DIC technique consists in identifying specific pattern at the sample surface and to follow it during the whole deformation. DIC gives access to the displacement field and strain fields can be obtained assuming some hypotheses [35].

3. Results and discussion

3.1. A multi-scale material

2D observation techniques, light and scanning electron microscopy give different information about the material. Fig. 2b shows that depending on the magnification and the technique, three different scales of the material microstructure can be defined.

- *Agglomerate scale* is the specimen scale. When mechanically loaded, it gives information on the mechanic behaviour through Force/Displacement curves and associated mechanical parameters (like Young's modulus or the absorbed energy).
- *Bead scale* is about the cork granulate that are millimetric. Porosities between beads, interfaces between granulates, beads orientation,... are parameters that could influence mechanisms at this scale.
- A cork bead is itself a cellular material. This is why a smaller scale exists. Indeed the size of cork cells is a few tens of micrometers. The *cell scale* is about how the cell walls deform themselves during a specific loading, cell geometry or the gaseous phase trapped inside,...

Hence the multi-scale structure of cork agglomerates, already broached for other polymeric foams is highlighted [23]. As each scale could influence each other and have an effect on the strain mechanisms, each one should be cautiously reported. It oriented the next analyses that are performed in this article.

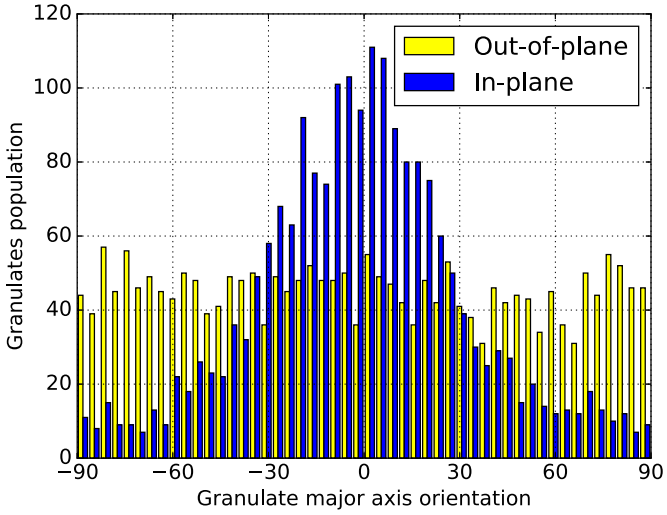

Fig. 8. Results from surface observation. Histograms of the granulates major orientation in cork agglomerates.

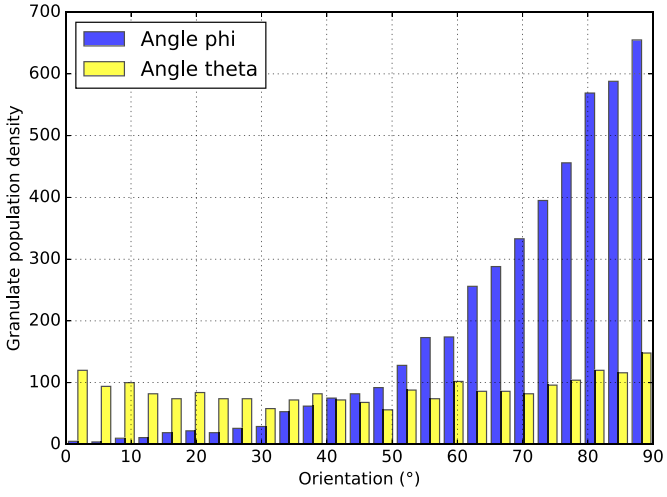

Fig. 9. Orientation of cork granulates obtained through X-ray microtomography.

3.2. Cork granulates

3.2.1. Transversal anisotropic orientation

Naked eye observations suffice to spot differences between in-plane and out-of-plane directions. In the out-of-plane direction, granulates keep the aspect they had before the process. Beads in the in-plane direction display an apparent elongation in the (Oy) direction. Observations made in the (Ox) or (Oy) directions are similar. Consequently the plane (Oxy) appears to be isotropic.

Picture analysis allowed to convert beads into ellipses. It confirmed In-plane granulates have mostly their major axis oriented at 0° while out-of-plane ones are randomly facing (Fig. 8).

Granulates orientation is also studied thanks to X-ray tomography. Cork beads spatial orientation is characterised by two angles ϕ and θ. Fig. 9 shows the value of these angles. θ values are equally distributed. On the contrary ϕ seems to lies essentially around 70 and 90°. This means that beads have a random orientation in the (Oxy) plane whereas in the (Oxz) or (Oyz) planes they tend to be aligned with the in-plane

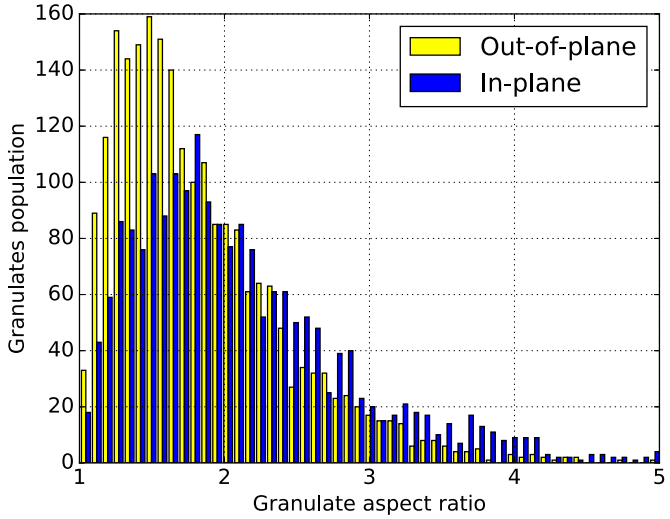

Fig. 10. Results of picture analysis. Distribution of the granulates aspect ratio.

directions. Light microscopy results are then supported by microtomography ones.

This observation can easily be linked to the process explained in the previous section. During the manufacturing process, the uniaxial compression likely orientate cork granulates in the (Oxy) plane.

3.2.2. Transversal anisotropic geometry

Dimensions considerations with optical microscopy show granulates observed in the out-of-plane direction tend to have an aspect ratio mostly between 1 and 2. Whereas the granulates observed in the In-plane direction have it between 2 and 3 (Fig. 10). Beads tend then to be rounder in the (Oxy) plane.

Tomography data were also helpful to better describe beads geometry.

Sphericity is presented in Fig. 11a. Cork granulates sphericity lies mostly between 0.4 and 0.8 which is a rather large spreading. The distribution can be associated with a normal distribution $f(x)$ expressed by the Eq. (4).

$$f(x) = \frac{1}{\sigma\sqrt{2\pi}} \cdot e^{-\frac{1}{2}(\frac{x-\mu}{\sigma})^2}. \quad (4)$$

The following parameters were used:

- x being the sphericity
- $\mu = 0.6$, mean of the distribution
- $\sigma = 0.07$, standard deviation of the distribution

It can be compared to beads dimensions obtained by surface observation. An ellipsoid of revolution with a = 0.45 mm (half major axis) and b = 0.22 mm (half minor axis) is an oblate spheroid (Fig. 11b). It would have a sphericity around 0.6. Once again 2D and 3D data match pretty well.

Thanks to the previous observations, it can be concluded that in addition to a specific orientation, cork beads present also an transversal anisotropic geometry. They can be in a first approximation assimilated with particles flattened in the transverse plane like oblate spheroid.

3.2.3. Beads organisation and interfaces

The microstructure of agglomerated cork demonstrates a random orientation of granulates in Fig. 12a. Each bead is characterised by cells grown in one direction (specified in Fig. 1).

Each granulate will then have a mechanical behaviour depending on it cells orientation in comparison to the load direction tensor just like natural cork [2].

SEM observations demonstrates thin interfaces hard to delimit between two beads (Fig. 12b). Resin was also uncertainly spotted with SEM observations but is revealed with the tomography analysis (Fig. 16). Indeed the largest whiter (thus denser) areas seem to correspond to the resin coating of cork beads.

3.2.4. Beads volume

The distribution of cork granulates volume is illustrated by Fig. 13. It represent more than 8000 beads in the VOI. The mean volume is around 9.9 10^{-2}mm^3. Its standard deviation is 9 10^{-2}mm^3. The distribution is thus rather wide. It may be compared with the volume of the same previous ellipsoid. Its volume is 9.5 10^{-2}mm^3.

Providing a appropriate post-treatment, microtomography is then a very powerful tool to study cork beads and to obtain valuable quantitative information. It allows to have distributed parameters to better describe the material at this scale.

3.3. Porosities

Porosities could be spotted on SEM pictures (Fig. 12). However no resin was trapped inside them.

On tomography pictures, porosities can also be spotted on three different plans. It appears they are not only due to the sample preparation for observations but are initially present in the material after the manufacturing process.

3.3.1. Porosities volume

The volume distribution of the porosities is shown in the Fig. 14. It is based on the results of more than 3000 porosities contained in the VOI. The mean volume stands around 0.027 mm^3 with a standard deviation of 0.024 mm^3

Globally they are smaller than cork beads but some of them have a significant volume near small cork beads volume.

3.3.2. Porosities shape

Fig. 15 shows the 3D reconstruction of the porosities. Each color is standing for one label.

The spatial visualisation of porosities demonstrate intricate shapes. Therefore usual shape descriptors could not be used here. The biggest porosity does not spread over the whole sample. Porosities are then not all interconnected.

Porosities between beads are often forgotten in cork agglomerate modelling due to the lack of insight about it. The surface analysis appears unsuitable to observe them. Microtomography appears here as the appropriate tool to study them. Their volume is large enough to have an influence on the mechanical behaviour and the associated mechanisms. The previous data will then be important for further modelling.

3.4. Cork cells

SEM and X-ray tomography allow both to observe cork agglomerates at a small scale and therefore to study cells contained in cork beads.

3.4.1. Cells geometry

Depending on the observation direction, the cell shape differs (Fig. 16). Rectangular and hexagonal sections are the most represented. This confirms the cork cell description made before thanks to SEM observations [2].

Furthermore corrugations described in the literature [2] could hardly be spotted. The resolution of the pictures taken could explain this. Voxel side being 2.5 μm large, corrugations would be to small.

3.4.2. Cells volume

Cork cells volume obtained by X-ray tomography are displayed in Fig. 17. It is based on the analysis of more than 1400 cells from in several

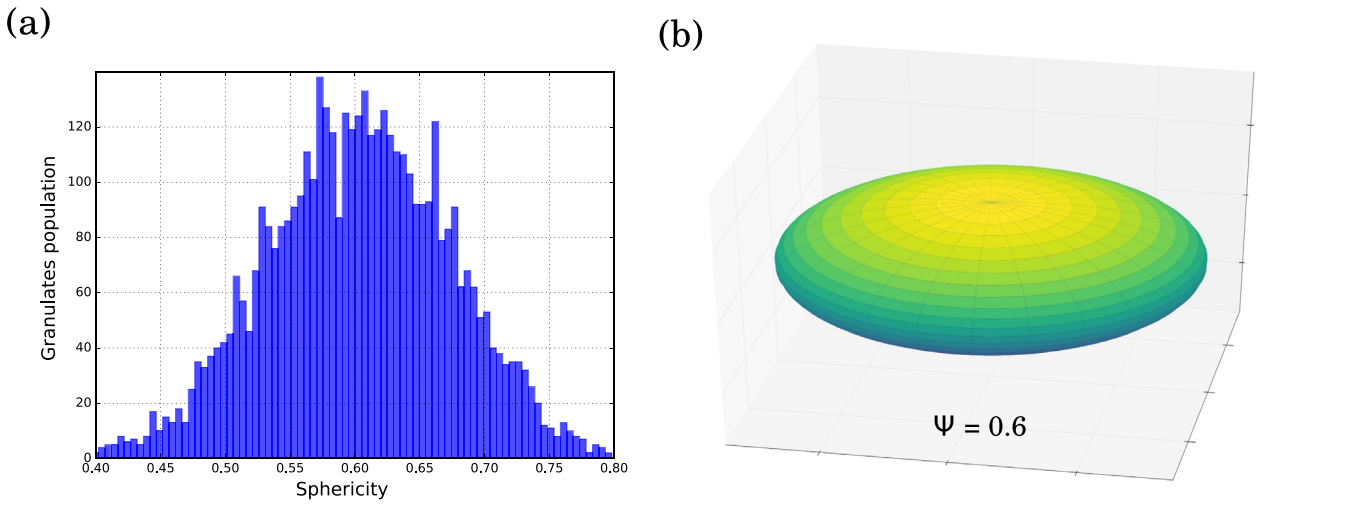

Fig. 11. 3D beads shape. (a) Results from computed tomography. Distribution of beads sphericity in a cork agglomerate obtained by uni-axial compression. (c) Oblate ellipsoid of revolution with a sphericity of 0.6.

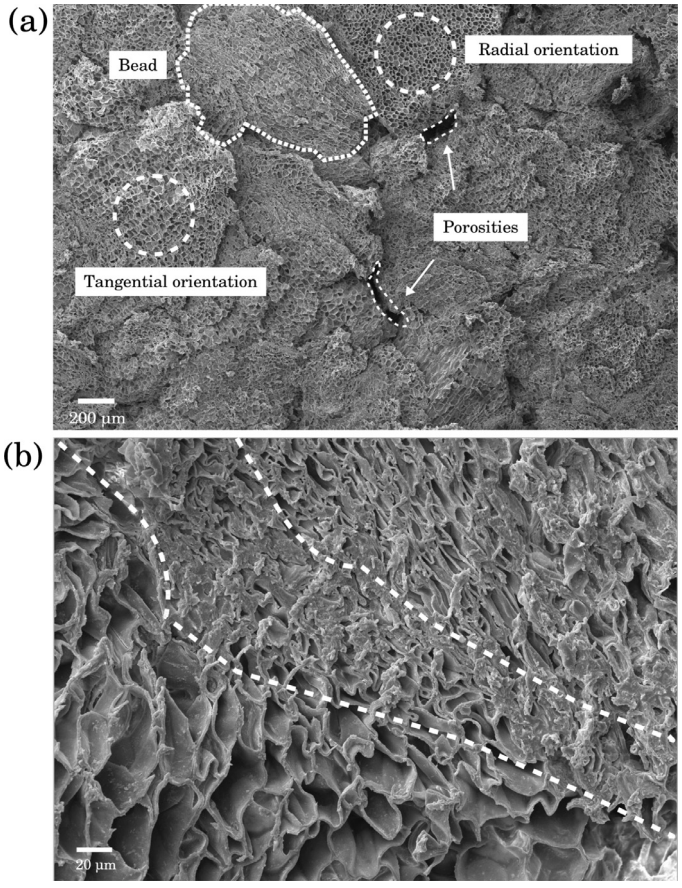

Fig. 12. SEM pictures of cork agglomerate at different scales. (a) Intricate microstructure.Random cells orientation encircled. Porosities highlighted by arrows. (b) Interface between two cork granulates. Approximative delimitation by dotted lines.

VOI contained in different beads. The mean cell volume is around 1 10^{-5} mm^3 with a standard deviation of 0.5 10^{-5} mm^3.

Comparison with 2D literature data was made by considering a simpler geometry than the real one. With the dimensions reported in [2] (h = 40 µm and l = 20 µm), for a circle-based cylinder, the cell volume would stand around 1.3 10^{-5} mm^3.

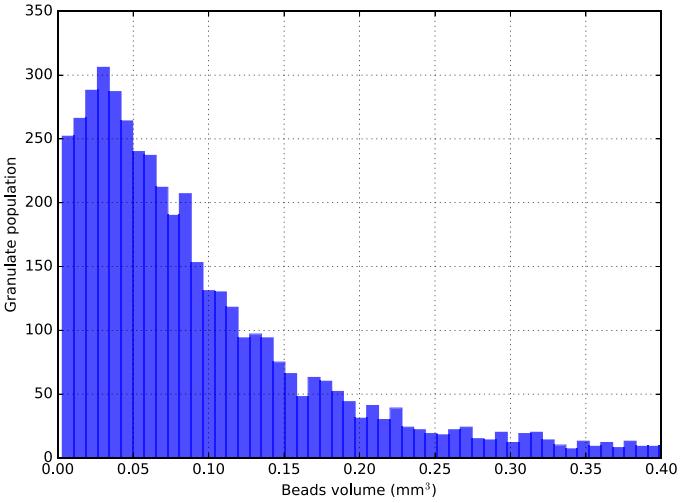

Fig. 13. Results from computed tomography. Distribution of beads volume in a cork agglomerate obtained by uni-axial compression.

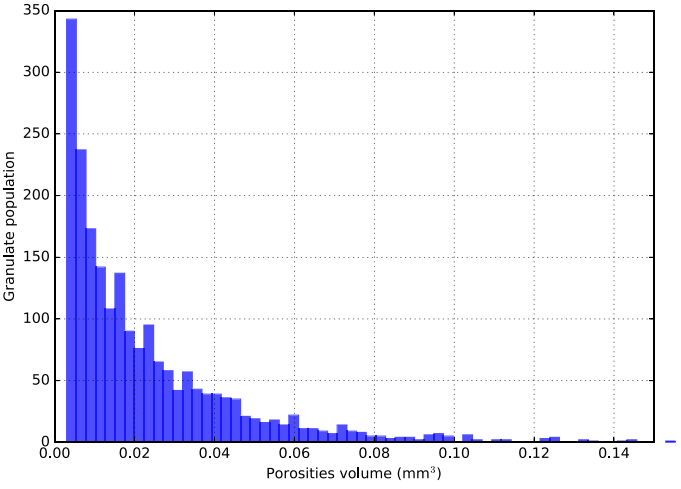

Fig. 14. Results from computed tomography. Distribution of porosities volume in a cork agglomerate obtained by uni-axial compression.

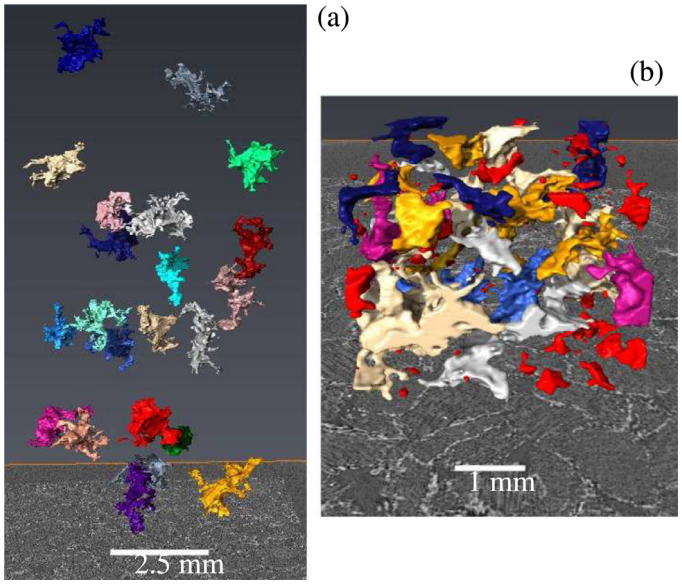

Fig. 15. 3D reconstruction of porosities between cork beads. (a) 40 biggest porosties in the whole sample. (b) All the porosties in a subvolume.

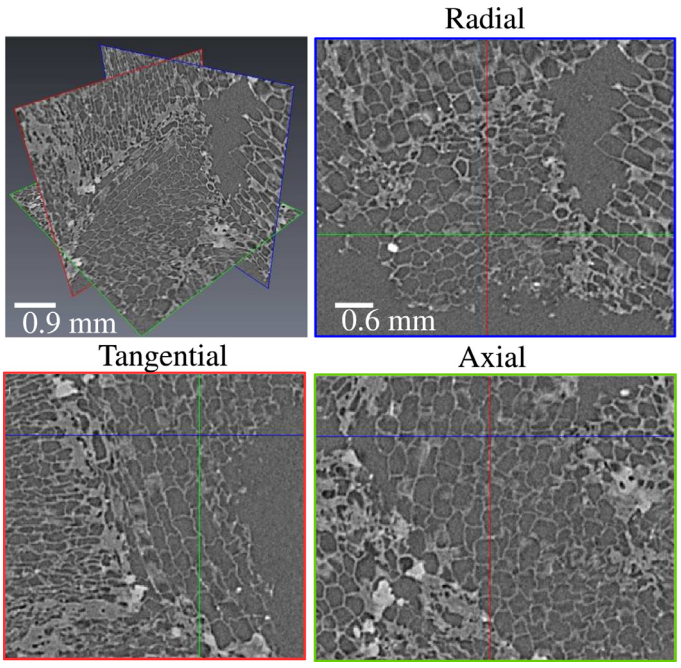

Fig. 16. Orthoslices of a subvolume obtained by computed tomography. The three main directions of cork cells are presented (radial, tangential and axial).

2D and 3D measures are then similar given the dimensional variation of cork cells depending on the environmental condition during the growth.

3.4.3. Cells deformation

As mentioned previously, SEM observations demonstrate that cork cells are often collapsed near interfaces (Fig. 18). For some beads, all the cells are deformed.

Three distinctive areas are highlighted here. The first is the interface with some resin. The following zone has cells that are totally collapsed. Finally far from the interface, cells are most of the time undamaged or at least only deformed.

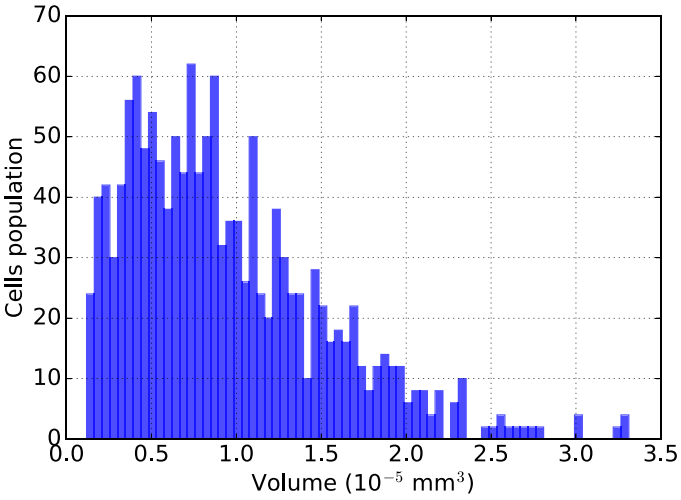

Fig. 17. Results from computed tomography. Cork cells volume distribution of cork agglomerate obtained by uni-axial compression.

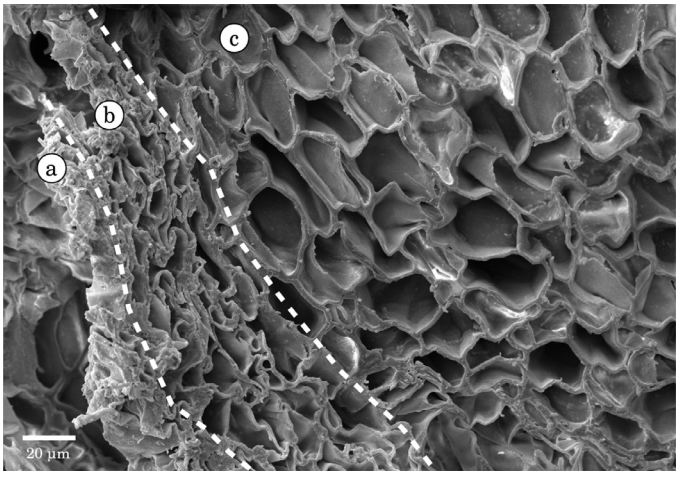

Fig. 18. SEM picture of the periphery of a cork bead (a) Interface. (b) Cork cell distortion in the vicinity of the interface. (c) Undamaged cells.

Hence some cells deformation is present at least from the manufacturing process. This pre-damaging probably influences strongly the strain mechanisms during a compressive loading.

3.5. Compressive behaviour

3.5.1. Foam-like behaviour

Fig. 19a presents the global compressive behaviour of agglomerated cork tested in the three directions. As already reported it demonstrates a foam-like distinctive compressive behaviour [8,9] and it seems to be an elastomeric foam [36]. Hence the three following main stages can be identified.

- Linear deformation (1)
- Plateau (2)
- Densification (3)

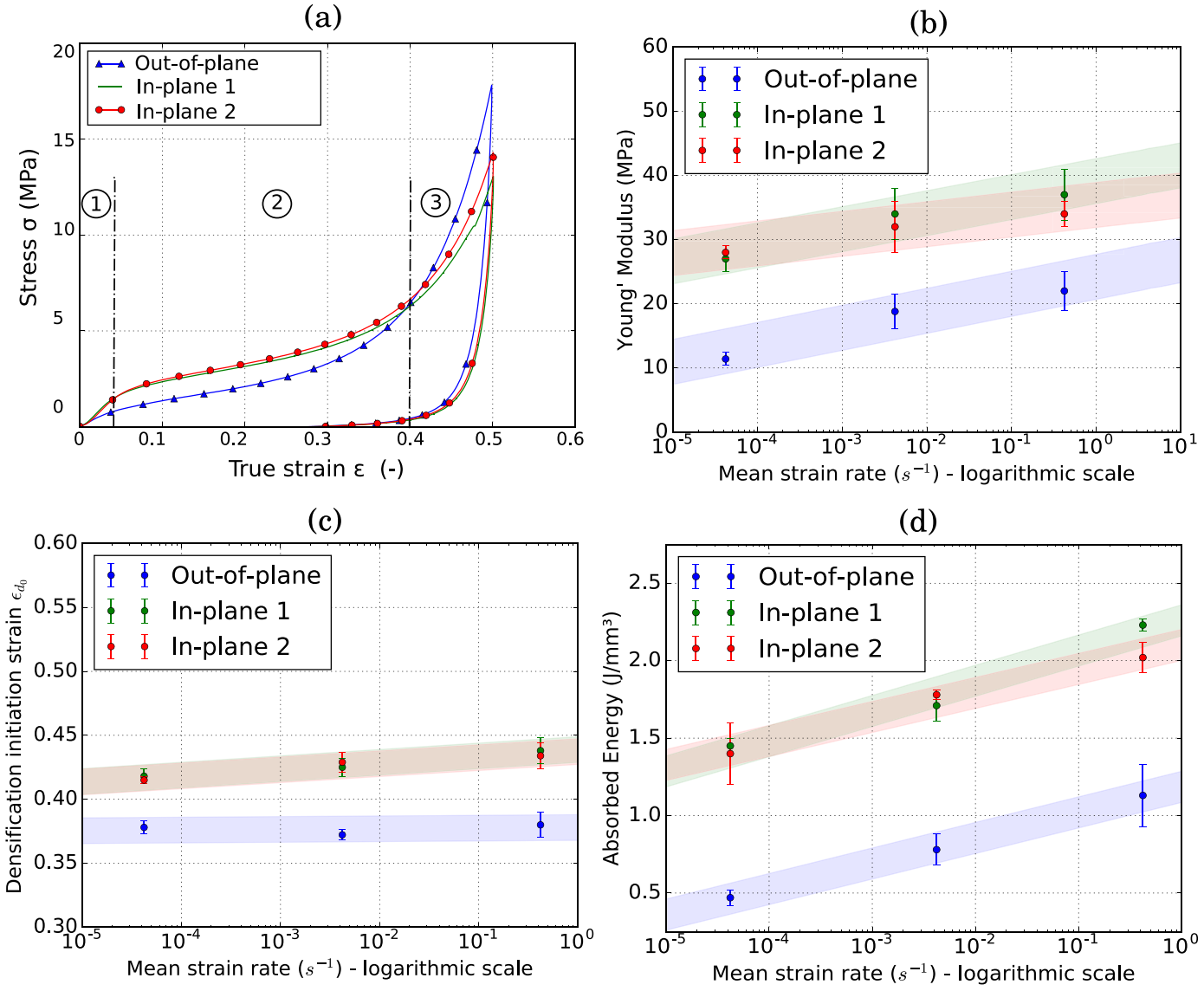

Fig. 19. Results of the compressive loadings. (a) A typical experimental compression curve of agglomerated cork tested in the 3 directions. (b) Young's modulus of cork agglomerates depending on the mean strain rate and the direction. (c) Densification initiation strain $\varepsilon = \varepsilon_{d_0}$ of cork agglomerates depending on the mean strain rate and the direction of sollicitation. (d) Absorbed energy at $\varepsilon = \varepsilon_{d0}$ of cork agglomerates depending on the mean strain rate and the direction of sollicitation.

3.5.2. Transverse anisotropic behaviour

From the three curves displayed in Fig. 19a, two main mechanical behaviours can be differentiated. Both in-plane directions appear stiffer than the out-of-plane direction. Furthermore they also reach densification stage after the out-of-plane direction.

Fig. 19b shows the evolution of Young's modulus for samples compressed in the out-of-plane or in-plane directions. Whereas two directions, in-plane 1 and in-plane 2, demonstrate a quasi-similar rigidity for the same solicitation speed, Young's modulus in the out-of-plane direction is around 60% lower.

The out-of-plane direction is then much less rigid and it seems the two in-plane directions are equivalent. This observation can be linked with previous observations made on the geometry and spatial orientation of cork beads. The collapsed cells near beads interfaces could also influence the direction stiffness as they are more oriented in the plane (Oxy). Indeed these interfaces are denser and stiffer than a simple cells row.

Cork agglomerates produced by uniaxial compression are then geometrically and mechanically anisotropic. This behaviour was not reported in previous articles [8–10]. However cork agglomerates studied there were half less dense that the one studied here. High density agglomerates could then tend to be less isotropic.

3.5.3. Visco-elasticity

Fig. 19b also demonstrates that the evolution of Young's modulus depends on the solicitation speed. An increase of the solicitation speed induces an increase of the Young's modulus.

Cyclic compressive curves of the two main directions of agglomerated cork are displayed in Fig. 20. Both curves display a visco-elastic hysteresis largely resulting from the viscosity of both cork cell walls [37] and the polymeric resin. The visco-elastic recovery upon unloading is small for the first cycle but increase once the plateau stage reached (starting from the second cycle).

Fig. 20 shows also visco-elastic recovery is higher for out-of-plane direction at short term. It is also true at long term. Indeed 2 months after the experiment, residual strain was respectively 0.067 ± 0.002 and 0.074 ± 0.003 for out-of-plane and in-plane directions.

Though intergranular failure was sometimes observed for in-plane samples just before the densification stage, cyclic curves indicate compression does not seem to cause major failure of cork cells just like for

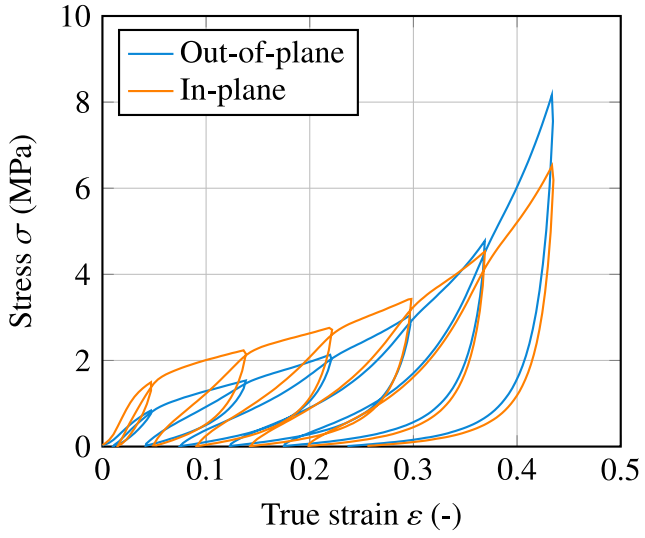

Fig. 20. Experimental cyclic strain-stress curve of agglomerated cork in different directions.

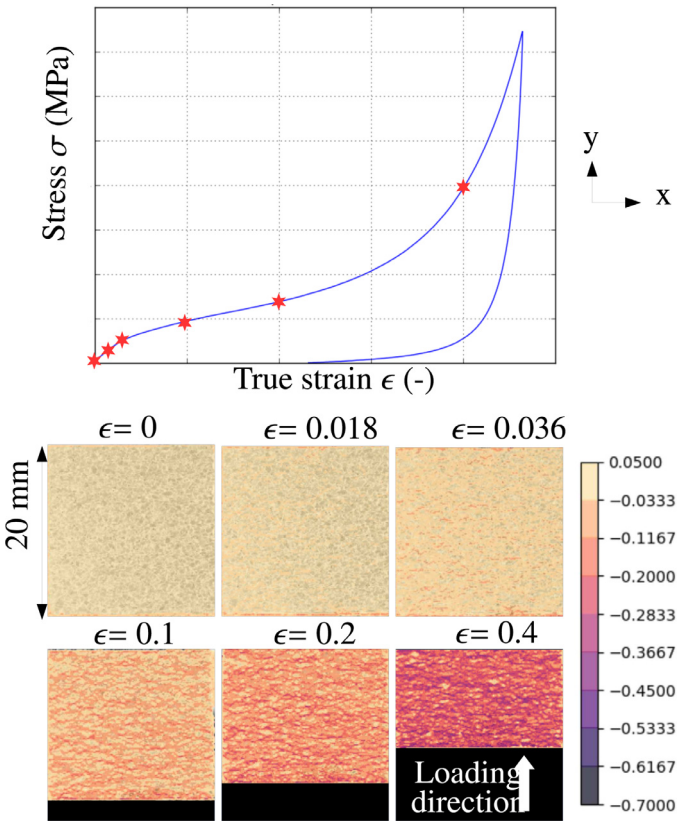

Fig. 21. YY-Strain map at several moments of the compression of cork agglomerate in the out-of-plane direction at 5 mm min^{-1}.

natural cork [22]. The capacity of the cells to deform without failure may be linked to the chemical composition of cork. The suberin macromolecule being a long-chain linear monomer [38], cell walls can buckled completly without fracture (Fig. 18). The recovery of the dimensions after stress removal can be associated with the unfolding of buckled cell walls. Permanent deformation is small and may be related to the cells collapsed near beads interface like observed in Fig. 18.

Hence cork agglomerates demonstrate a visco-elastic compressive mechanical behaviour. Natural cork was already reported having such behaviour [37]. So cork beads constituent material and resin are likely responsible for such behaviour as they are both polymers (or an assemblage of several polymers).

3.5.4. Energy absorption properties

The presence of a stress plateau during a compression loading induces interesting properties for energy absorption applications [36].

According to Fig. 19c, densification happened around $\varepsilon = 0.42$ and $\varepsilon = 0.38$ when the sample is tested respectively in the in-plane and out-of-plane direction. Considering the manufacturing process, this difference of densification strain between tested directions is likely caused by the fact agglomerated cork was already compressed a first time in the out-of-plane direction. Some cork cells would then already have buckled in this direction.

Failure happened for some samples compressed in the in-plane direction. The η computation indicates this failure was always around the densification initiation strain.

The solicitation speed does not seem to have a major influence on ε_{d0} (Fig. 19c). On the contrary, absorbed energy increases with the speed solicitation (Fig. 19d) and is higher for the In-plane direction. Energy absorbed in the in-plane direction varies from 1.5 to 2 J mm^{-3} and from 0.5 to 1 J mm^{-3} in the out-of-plane direction. In-plane direction absorbs more energy likely because it is stiffer than out-of-plane direction and it densifies at a higher strain [36].

The relative density ρ^*/ρ_s of this material is around 0.34 which is quite high for a cellular material. Energy absorption would then be dominated by cell-wall behaviour. The compression of the gas within the cells would be negligible at quasi-static compressive loadings [36].

Previous works took interest in the absorbed energy too. However it was calculated at the beginning of the densification but at high strains [8] or at several strain through the compression cycle [9]. The absorbed energy was much lower (around 300 J mm^{-3} at the densification strain [9]) than for the material studied here. Yet each agglomerated cork has its own features. A polyurethane resin was often used. The proportions were also differents. Finally the material density was often lower (around 0.2 [8]). All these divergent points can then explain the discrepancies between absorbed energies obtained.

Agglomerated cork seems suited for protective applications has it appeared to be able to convert kinetic energy into energy of some other sort whilst keeping the load relatively low thanks to the plateau stage (around 4 MPa before densification).

3.5.5. Strain mechanisms

In Fig. 21, the evolution of the strain in the loading direction is shown. Until the beginning of the plateau, strain seems quite homogeneous. However once the compression reaches the plateau, at $\varepsilon = 0.036$, higher strain bands appear at the sample surface whereas the rest of the surface remain almost intact. Afterwards strain increases in these bands whereas the sample globally deforms.

These kind of localisations are called *localisation bands*. Mostly multi-scale foams demonstrate such strain behaviour [23]. Such localisations have already been observed for agglomerated cork compressed at quasi-static or dynamic regime [12].

Such mechanisms can be related to the strain/stress curve. At first the deformation is linear and homogeneous which could be associated with an elastic behaviour.

Once the stress is high enough at a specific place, local buckling of cell walls starts and localisation bands appear. Hence the plateau corresponds to the propagation of cork cells buckling, bead by bead, Gibson and Ashby [36]. Strain propagation could be explained by considering either a bead or cell with lower mechanical properties, so-called "*size effect*", or a more solicited bead or cell, "*multi-scale structure effect*" [23].

For higher strain ($\varepsilon \geq \varepsilon_{d0}$), once almost every cell is collapsed, the densification stage is reached. The material then behaves as a bulk one. That is why stress increases faster. All the scales of cork agglomerates presented in this article could play a role in the strain mechanisms of this

material. These mechanisms can be therefore considered as multi-scale. Further work is though needed to be able to better describe it.

4. Conclusions & perspectives

Cork agglomerate has been used for decades. However its microstructure and mechanical behaviour is still not fully understood. This study aimed at initiating discussions about the multi-scale and complexe material microstructure and its influence on the mechanical behaviour.

Optical and scanning-electron microscopy techniques were used to obtain a first micro-structural description of the surface. Beads angle and shape factor permitted to notice the geometrical transverse anisotropy of agglomerated cork produced by uni-axial compression.

X-ray microtomography appeared to be very appropriate to better describe this material in 3D. Two different scales were studied : beads and cells. It brought additional information and allowed to confirm previous 2D observations by capturing architectural information (cell volume distribution, cell wall defects, porosities size,...) and thanks to a non-intrusive process. This quantified study could be considered as a new input for models which would better describe the specific behaviour of cork agglomerates.

Compression tests demonstrated that the specific anisotropic geometry led to a transverse anisotropic mechanical behaviour. In-plane direction is stiffer, absorbs more energy, densifies at higher strains and has a lower visco-elastic recovery than out-of-plane direction.

High strain heterogeneities were highlighted during compressive loading in a quasi-static regime thanks to DIC. There were identified as localisation bands.

Future work will focused on a precise explanation of these localisations and more widely on the strain and damage mechanisms at higher strain rates.

Acknowledgements

The authors gratefully acknowledge Liege HPK for providing specimens. This work was performed in the framework of the LIAMA project (supported by Safran Power Unit and Région Nouvelle Aquitaine).

Digital Image Analysis was performed using the free software Pydic running with Python developed by Damien André and the authors thank him for it.

References

[1] L. Gil, New cork-based materials and applications, Materials (2) 625–637. doi:10.3390/ma8020625.
[2] L.J. Gibson, K.E. Easterling, M.F. Ashby, The structure and mechanics of cork, Proc. R. Soc. A Math. Phys. Eng. Sci. 377 (1769) (1981) 99–117, doi:10.1098/rspa.1981.0117.
[3] L. Gil, Cork composites: a review, Materials (3) 776–789. doi:10.3390/ma2030776.
[4] F.C. Potes, J.M. Silva, P.V. Gamboa, Development and characterization of a natural lightweight composite solution for aircraft structural applications, Compos. Struct. 430–440. doi:10.1016/j.compstruct.2015.10.034.
[5] M.M. Mateus, J.M. Bordado, R.G. dos Santos, Ultimate use of cork unorthodox and innovative applications, Ciência & Tecnologia dos Materiais 29 (2) (2017) 65–72, doi:10.1016/j.ctmat.2016.03.005.
[6] H. Pereira, E. Ferreira, Scanning electron microscopy observations of insulation cork agglomerates, Mater. Sci. Eng. A 111 (C) (1989) 217–225, doi:10.1016/0921-5093(89)90215-3.
[7] H. Pereira, Variability of the chemical composition of cork, BioResources 8 (2) (2013) 2246–2256, doi:10.1016/B978-044452967-1/50005-4.
[8] R. Jardin, F. Fernandes, A. Pereira, R. Alves de Sousa, Static and dynamic mechanical response of different cork agglomerates, Mater. Des. 68 (2015) 121–126, doi:10.1016/j.matdes.2014.12.016.
[9] P.T. Santos, S. Pinto, P.A. Marques, A.B. Pereira, R.J. Alves de Sousa, Agglomerated cork: a way to tailor its mechanical properties, Compos. Struct. 178 (2017) 277–287, doi:10.1016/j.compstruct.2017.07.035.
[10] C.P. Gameiro, J. Cirne, G. Gary, Experimental study of the quasi-static and dynamic behaviour of cork under compressive loading, J. Mater. Sci.(12) 4316–4324. doi:10.1007/s10853-006-0675-6.
[11] S. Sanchez-Saez, S.K. García-Castillo, E. Barbero, J. Cirne, Dynamic crushing behaviour of agglomerated cork, Mater. Des.(1980–2015)743–748. doi:10.1016/j.matdes.2014.09.054.
[12] M. Sasso, E. Mancini, G. Chiappini, F. Sarasini, J. Tirillò, Application of DIC to static and dynamic testing of agglomerated cork material, 2018, doi:10.1007/s11340-017-0369-9.
[13] A. Lagorce-Tachon, F. Mairesse, T. Karbowiak, R.D. Gougeon, J.-P. Bellat, T. Sliwa, J.-M. Simon, Contribution of image processing for analyzing the cellular structure of cork, J. Chemom. 8 (July) (2017), doi:10.1002/cem.2988.
[14] A. Lagorce-Tachon, T. Karbowiak, C. Loupiac, A. Gaudry, F. Ott, C. Alba-Simionesco, R.D. Gougeon, V. Alcantara, D. Mannes, A. Kaestner, E. Lehmann, J.P. Bellat, The cork viewed from the inside, J. Food Eng. 149 (2015) 214–221, doi:10.1016/j.jfoodeng.2014.10.023.
[15] A. Brunetti, R. Cesareo, B. Golosio, P. Luciano, A. Ruggero, Cork quality estimation by using {Compton} tomography, Nucl. Instrum. Methods Phys. Res. Sect. B Beam Interact. Mater. Atoms 196 (2002) 161–168, doi:10.1016/S0168-583X(02)01289-2.
[16] V. Oliveira, P. Lopes, M. Cabral, H. Pereira, Influence of cork defects in the oxygen ingress through wine stoppers: insights with X-ray tomography, J. Food Eng. (2015), doi:10.1016/j.jfoodeng.2015.05.019.
[17] V. Oliveira, J. Van Den Bulcke, J. Van Acker, T. De Schryver, H. Pereira, Cork structural discontinuities studied with X-ray microtomography, Holzforschung (2016), doi:10.1515/hf-2014-0245.
[18] V.R. Donepudi, R. Cesareo, A. Brunetti, Z. Zhong, T. Yuasa, T. Akatsuka, T. Takeda, G.E. Gigante, Cork embedded internal features and contrast mechanisms with DEI using 18, 20, 30, 36, and 40 kev synchrotron x-rays, Res. Nondestruct. Eval. 21 (3) (2010) 171–183, doi:10.1080/09349847.2010.493990.
[19] E. Maire, L. Babout, J.Y. Buffiere, R. Fougeres, Recent results on 3D characterisation of microstructure and damage of metal matrix composites and a metalic foam using X-ray tomography, Mater. Sci. Eng. A 319–321 (2001) 216–219, doi:10.1016/S0921-5093(01)00924-8.
[20] E. Maire, A. Fazekas, L. Salvo, R. Dendievel, S. Youssef, P. Cloetens, J.M. Letang, X-ray tomography applied to the characterization of cellular materials. Related finite element modeling problems, Compos. Sci. Technol. 63 (16) (2003) 2431–2443, doi:10.1016/S0266-3538(03)00276-8.
[21] T. Dillard, F. N'Guyen, E. Maire, L. Salvo, S. Forest, Y. Bienvenu, J.D. Bartout, M. Croset, R. Dendievel, P. Cloetens, 3D quantitative image analysis of open-cell nickel foams under tension and compression loading using X-ray microtomography, Philos. Mag. (2005), doi:10.1080/14786430412331331916.
[22] H. Pereira, The rationale behind cork properties: a review of structure and chemistry, BioResources (2015), doi:10.15376/biores.10.3.Pereira.
[23] P. Viot, D. Bernard, Multi-scale foam behaviour characterisation, Comput. Methods Exp. Mater. Charact. III I (2007) 197–206, doi:10.2495/MC070201.
[24] S.P. Silva, M.A. Sabino, E.M. Fernandes, V.M. Correlo, L.F. Boesel, R.L. Reis, Cork: properties, capabilities and applications, Int. Mater. Rev. 50 (6) (2005) 345–365, doi:10.1179/174328005X41168.
[25] A. Lagorce-Tachon, T. Karbowiak, D. Champion, R.D. Gougeon, J.P. Bellat, Mechanical properties of cork: effect of hydration, Mater. Des. 82 (2015) 148–154, doi:10.1016/j.matdes.2015.05.034.
[26] E. Maire, J.Y. Buffière, L. Salvo, J.J. Blandin, W. Ludwig, J.M. Létang, On the Application of X-ray microtomography in the field of materials science, Adv. Eng. Mater. 3 (8) (2001) 539, doi:10.1002/1527-2648(200108)3:8<539::AID-ADEM539>3.0.CO;2-6.
[27] O.B. Olurin, M. Arnold, C. Krner, R. Singer, The investigation of morphometric parameters of aluminium foams using micro-computed tomography, Mater. Sci. Eng. A (2002), doi:10.1016/S0921-5093(01)01809-3.
[28] M. Coster, J.-L. Chermant, Precis d'Analyse d'Images, Éditions du CNRS, Paris, 1985.
[29] J. Serra, Advances in mathematical morphology: segmentation, 2008, doi:10.1016/S1076-5670(07)00004-3.
[30] C. Lantuejoul, F. Maisonneuve, Geodesic methods in quantitative image analysis, Pattern Recognit. (1984), doi:10.1016/0031-3203(84)90057-8.
[31] F. Meyer, S. Beucher, Morphological segmentation, J. Vis. Commun. Image Represent. (1990), doi:10.1016/1047-3203(90)90014-M.
[32] Y. Sun, B. Amirrasouli, S.B. Razavi, Q.M. Li, T. Lowe, P.J. Withers, The variation in elastic modulus throughout the compression of foam materials, Acta Materialia (2016), doi:10.1016/j.actamat.2016.03.003.
[33] Q.M. Li, I. Magkiriadis, J.J. Harrigan, Compressive strain at the onset of densification of cellular solids, J. Cell. Plast. (2006), doi:10.1177/0021955X06063519.
[34] M. Avalle, G. Belingardi, R. Montanini, Characterization of polymeric structural foams under compressive impact loading by means of energy-absorption diagram, Int. J. Impact Eng. (2001), doi:10.1016/S0734-743X(00)00060-9.
[35] Hild Francois, J.-l. Prensier, Annexe : algorithme de calcul de corrélation d ' images numériques, Technical Report, ENS Cachan, 2004.
[36] L.J. Gibson, M.F. Ashby, Cellular Solids: Structure and Properties, cambridge, Cambridge University Press, Oxford, 1997.
[37] J.F. Mano, The viscoelastic properties of cork, J. Mater. Sci. 37 (2) (2002) 257–263, doi:10.1023/A:1013635809035.
[38] H. Pereira, Cork: Biology, Production and Uses, Elsevier B.V., Oxford, 2007, doi:10.1007/978-3-319-23880-7_5.